try and Polarized Light," Chap. 4, North-Holland, Amsterdam (1977).
26. D. E. Aspnes and J. B. Theeten, *This Journal*, **127**, 1359 (1980); *Phys. Rev. Lett.*, **43**, 1046 (1979).
27. F. L. McCracken, Technical Note 479, National Bureau of Standards (1969).
28. E. Taft and L. Cordes, *This Journal*, **126**, 131 (1979).
29. R. J. Archer, *J. Opt. Soc. Am.*, **52**, 970 (1962).
30. E. D. Palik, J. W. Gibson, R. T. Holm, M. Hass, M. Braunstein, and B. Garcia, *Appl. Opt.*, **17**, 1776 (1978).
31. P. F. Schmidt and W. Michel, *This Journal*, **104**, 230 (1957).
32. J. D. E. Beynon, G. G. Bloodworth, and I. M. McLeod *Solid State Electron.*, **16**, 309 (1973).
33. S. R. Morrison, "Electrochemistry at Semiconductor and Oxidized Metal Electrodes," Chap. 2, Plenum Press, New York (1980).
34. P. F. Schmidt and J. D. Ashner, *This Journal*, **118**, 325 (1971).
35. A. G. Revesz, *J. Non-Cryst. Solids*, **11**, 309 (1973).
36. V. Brusic, in "The Anodic Behavior of Metals and Semiconductor Series; Oxides and Oxide Films," J. W. Diggle, Editor, p. 1 and references therein, Marcel Dekker, New York (1972).
37. W. A. Pliskin and H. S. Lehman, *This Journal*, **112**, 1013 (1965).
38. W. W. Harvey and J. Kruger, *Electrochim. Acta*, **16**, 2017 (1971).
39. B. MacDougall and M. Cohen, in "Passivity of Metals," R. P. Frankenthal and J. Kruger, Editors, p. 827, The Electrochemical Society Softbound Proceedings Series, Princeton, NJ (1978).
40. W. H. Brattain and C. G. B. Garrett, *Bell. Tel. Syst. J.*, **34**, 129 (1955).
41. H. Gerischer, *Surf. Sci.*, **18**, 97 (1969).
42. S. R. Morrison, "Electrochemistry at Semiconductor and Oxidized Metal Electrodes," Chap. 3, Plenum Press, New York (1980).
43. M. Seipt, *Z. Naturforsch.*, **14a**, 926 (1959).
44. J. F. Dewald, "Semiconductors," B. Hannay, Editor, p. 727, Reinhold, New York (1959).
45. M. Green, in "Modern Aspects of Electrochemistry," J. O'M. Bockris, Editor, p. 343, Butterworths, London (1959).
46. P. Lorbeer and W. J. Lorenz, *Corros. Sci.*, **21**, 79 (1981).
47. D. R. Turner, *This Journal*, **103**, 252 (1956).
48. Y. J. Van der Meuken, *ibid.*, **119**, 530 (1972).
49. J. R. Ligenza, *J. Phys. Chem.*, **65**, 2011 (1961).
50. P. F. Schmidt and A. E. Owen, *This Journal*, **111**, 682 (1964).
51. A. G. Revesz, *Phys. Status Solidi*, **57a**, 657 (1980); **58a**, 107 (1980).

# Polycrystalline Silicon Micromechanical Beams

**R. T. Howe and R. S. Muller**

*Department of Electrical Engineering and Computer Sciences, and the Electronics Research Laboratory, University of California, Berkeley, California 94720*

ABSTRACT

Using the conventional MOS planar process, miniature cantilever and doubly supported mechanical beams are fabricated from polycrystalline silicon. Poly-Si micromechanical beams having thicknesses of 230 nm to 2.3 $\mu$m and separated by 550 nm to 3.5$\mu$m from the substrate are made in a wide range of lengths and widths. Two static mechanical properties are investigated: the dependences of maximum free-standing length and beam deflection on the thickness of the beam. By annealing the poly-Si prior to beam formation, both of these properties are improved. Nonuniform internal stress in the poly-Si is apparently responsible for the beam deflection.

A novel method is described for making cantilever and doubly supported micromechanical beams from polycrystalline silicon (poly-Si). Only two masking steps are needed, as illustrated in Fig. 1. The first step, Fig. 1a, opens windows in an oxide layer grown or deposited on the silicon wafer. Next, poly-Si is deposited and plasma-etched in a second masking step, leaving the cross-section of Fig. 1b. Immersing the wafer in buffered HF removes all oxide, undercutting the poly-Si layer and creating the cantilever beam, illustrated in Fig. 1c. Doubly supported beams, Fig. 1d, are made by including a second oxide window at the opposite end of the beam.

For several reasons, this technique for making poly-Si beams is a useful addition to silicon micromechanics technology. First, poly-Si is widely used in MOS integrated circuits and a well-developed technology exists for depositing it in thin films and controlling its electrical properties. Second, the piezoresistivity of poly-Si could be utilized in integrated sensors; a monolithic pressure transducer based on a poly-Si membrane has already exploited this property (1). Finally, the simple fabrication process outlined above uses only conventional MOS planar technology which greatly simplifies the integration of micromechanical beams and MOS circuitry. This compatibility with standard processing contrasts with beam fabrication techniques based on anisotropic etchants (2, 3). MOS transistors have been fabricated adjacent to miniature cantilever beams made by anisotropic etching of the epitaxial silicon underlying a patterned, etch-resistant layer (4). However, the use of an epitaxial layer and anisotropic etchants in this earlier work represents a substantial departure from the conventional MOS process.

To assess fully the potential of this new technique, both the static and dynamic mechanical properties of poly-Si beams should be determined. This study investigates the static properties by fabricating poly-Si beams having a wide range of dimensions. In particular, the dependences of maximum free-standing beam length and cantilever beam deflection on the thickness of the beam are determined. A more complex process,

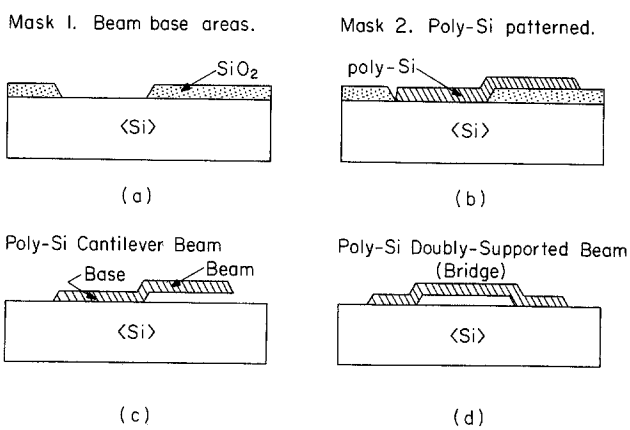


Fig. 1. Poly-Si microbeam fabrication

Key words: mechanics, membrane, integrated circuits.

including an MOS circuit for sensing the beam vibrations, is being developed to investigate the dynamic properties. Results for Young's modulus and fatigue characteristics of poly-Si micromechanical beams will be reported later.

## Fabrication

We now describe poly-Si beam fabrication in more detail. In order to minimize stress concentration during flexing, the step in the poly-Si beam, shown in Fig. 1c, should be gradual. This consideration makes it desirable to have a tapered oxide-window edge. Two process runs with different oxide-layer compositions are made. Figure 2 illustrates the resulting oxide-window edges, as observed with a scanning-electron microscope. In the first run, the oxide layer is one-third wet thermal $SiO_2$ and two-thirds CVD $SiO_2$. The latter is densified at 975°C for 20 min after deposition. In the second run, a more gradual edge profile is obtained with an oxide layer consisting of 10% thermal $SiO_2$ and 90% phosphosilicate glass (about 8.75% phosphorus content). The thin, rapidly etching surface layer needed for a tapered oxide-window edge is created by a low-energy argon implant (5). The phosphosilicate glass is densified at 1100°C for 20 min prior to the argon implant.

The poly-Si thin film is deposited by pyrolysis of silane at a temperature of 640°C and a pressure of 600 mTorr, resulting in a deposition rate of approximately 10 nm $min^{-1}$ and a grain size of 30-50 nm (6). No high temperature processing is done after poly-Si deposition, except for one sample having a 3.5 μm oxide layer and a 2.0 μm poly-Si layer. In this case, the wafer is annealed at 1100°C in $N_2$ for 20 min prior to immersion in buffered HF.

In order to establish the dimensional limitations on poly-Si beams, a wide variety of beams have been fabricated in the two process runs. Several combinations of oxide and poly-Si thicknesses, listed in Fig. 3, were used. The first-run cantilevers are T-shaped with the cross bar at the free end (cf. Fig. 5). They range in length from 25 to 200 μm, with various widths. Both simple cantilevers (without cross bars) and bridges are included on second-run masks. These cantilevers are 25-400 μm long, and the bridges range from 100 to 500 μm in length. Several series of beams are included in which length or width is varied with the other dimension being held constant. All cantilevers have bases as long as the beams (cf. Fig. 1c) except for one second-run series in which the base length has been progressively shortened.

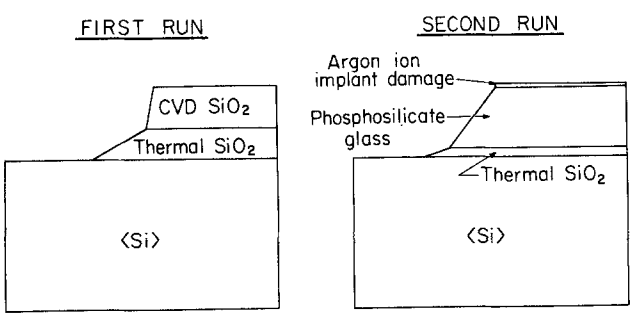


Fig. 2. Oxide-window edges for both process runs

Thickness of oxide supporting layer

| Thickness of poly-Si beam | 550 nm | 1.7 μm | 2.0 μm | 3.5 μm |
|---|---|---|---|---|
| 230 nm | ○ | ○ | | ○ |
| 800 nm | ○ | ○ | | ○ |
| 1.2μm | | | □ | |
| 2.0μm | | ○ | | ○ |
| 2.3μm | | | □ | |

□: First run, Cantilevers.
○: Second run, Cantilevers & bridges.

Fig. 3. Poly-Si and oxide thicknesses used to fabricate beams

## Results

All of the combinations of oxide and poly-Si thicknesses listed in Fig. 3 produce some free-standing poly-Si beams. No cracking is seen at the step in the poly-Si, even for first-run cantilevers, in which the oxide-window edge is very abrupt (cf. Fig. 2). Long bases for poly-Si cantilevers are not needed, as demonstrated by the series of cantilevers with shortened bases. For all the combinations enumerated in Fig. 3, a 5 μm long base is sufficient for a free-standing cantilever which is 45 μm long and 20 μm wide.

Scanning-electron micrographs of four representative cantilevers are shown in Fig. 4. These beams are 60 μm long, 800 nm thick, and are 3.5 μm above the silicon substrate. Widths range from 25 μm for the leftmost beam to 60 μm for the rightmost one. The bases are at the lower right, and the steps in the poly-Si are clearly visible. We will discuss later the upward deflection of these beams which can be seen in Fig. 4.

An apertured poly-Si beam is shown in Fig. 5. The T-shaped cantilever is 100 μm long, 40 μm wide, 2.3 μm thick, and has a 2 μm gap between beam and substrate. No special care in rinsing or drying the wafer after undercutting the beams is taken for the first process run, which produced this beam. An apertured cantilever is of interest for certain sensor applications (7) and the beam shown in Fig. 5 demonstrates the feasibility of this concept.

Very thin poly-Si layers can cover large oxide steps and form free-standing micromechanical beams, as can be seen in Fig. 6. The cantilever in Fig. 6 is 25 μm long and only 230 nm thick with a 3.5 μm separation be-

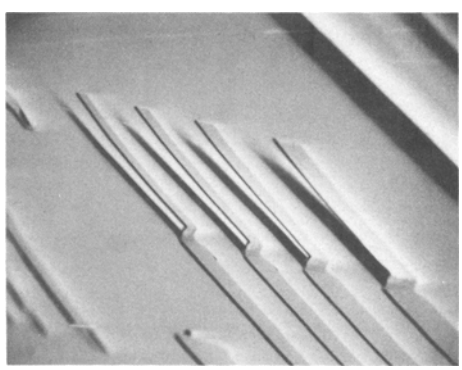

Fig. 4. Poly-Si cantilevers: 60 μm long, 800 nm thick, with a 3.5 μm beam-substrate gap.

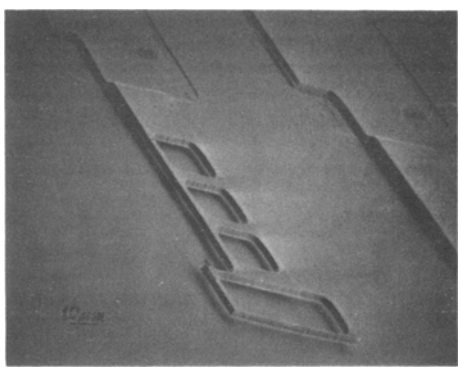

Fig. 5. Apertured poly-Si beam: 100 μm long, 2.3 μm thick, with a 2 μm beam-substrate gap.

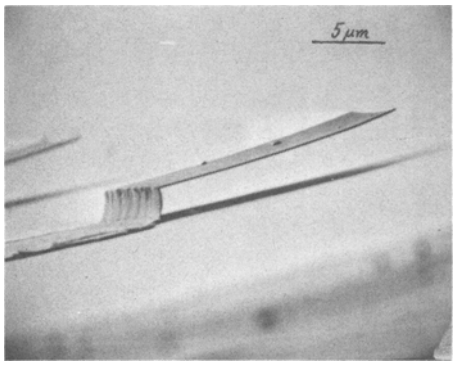


Fig. 6. Thin poly-Si cantilever: 25 μm long, 230 nm thick, with a 3.5 μm beam-substrate separation.

tween beam and substrate. Some debris from scribing is visible on top of the beam and variations in the oxide-window edge have been reproduced in the thin poly-Si layer. This beam is from a process run in which the wafers are dipped in water after etching in buffered HF and dried under an infrared lamp.

Beyond a certain length, both cantilevers and bridges are observed either to deflect downward and ultimately contact the substrate or to deflect upward severely. This limiting length, defined as the maximum free-standing length $L_m$, is repeatable from die to die within a wafer. It is observed that $L_m$ depends strongly on the thickness of the beam. Width and beam-substrate gap do not have a repeatable influence on $L_m$ in the first two process runs. However, the maximum free-standing length is probably sensitive to processing details, such as the poly-Si deposition conditions and the oxide etching procedure. The results obtained here are, nonetheless, useful as guidelines for evaluating poly-Si beam technology.

In order to determine $L_m$ as a function of thickness for these poly-Si beams, a series of 15 μm wide cantilevers and bridges with increasing lengths were investigated. The average of the lengths of the longest repeatably free-standing beam and the next longer beam is an empirical estimate of $L_m$. This measurement is plotted against beam thickness for both cantilevers and bridges in Fig. 7. The curves in Fig. 7 are empirical fits to the data and are given by

$$L_m = \begin{cases} \sqrt{4500t} & \text{for cantilevers} \\ \sqrt{11{,}500t} & \text{for bridges} \end{cases} \quad [1]$$

where $t$(μm) is the beam thickness and $L_m$(μm) is the maximum free-standing beam length. Cantilevers or bridges located above the relevant curve in Fig. 7 cannot be used, since they will touch the substrate or be severely deflected. Note that the sample which is annealed before the beams are undercut shows substantial increases in maximum free-standing lengths for both cantilevers and bridges, as indicated by the filled symbols in Fig. 7. As mentioned above, these results are process-dependent and therefore should be considered as first-order guidelines.

Cantilever poly-Si beams with lengths less than $L_m$ deflect upward, away from the substrate, as can be seen in Fig. 4 and 6. Scanning-electron micrographs indicate that the deflection curve is parabolic for small tip deflections (less than one-tenth of the beam length). In addition, the tip deflections of cantilevers of constant thickness are proportional to the squares of their lengths. These results suggest the presence of an internal bending-moment $M_i$ in the poly-Si beams, since a tip deflection $y$ given by

$$y = \frac{6M_i L^2}{E_Y t^3} \quad [2]$$

where $L$ is the cantilever's length, $t$ its thickness, and $E_Y$ its Young's modulus, is predicted for this case (8). The physical origin for the bending moment $M_i$ is discussed later.

It is convenient to use the quantity $(y/L^2)$ to characterize beam deflection, since it is independent of beam length. The inset in Fig. 8 defines the tip deflection measurement, and the plot shows the variations of $(y/L^2)$ with beam thickness for both first- and second-run cantilevers. According to Fig. 8, thicker beams deflect less at a given length, as one would expect. As before, annealing the sample affects the static mechanical properties of poly-Si beams. This is indicated by the filled circle in Fig. 8. In contrast to the unannealed sample of the same thickness no measurable deflection is observed for cantilevers shorter than $L_m$ on the annealed wafer. These cantilever deflection results also are sensitive to processing details and should be interpreted accordingly.

## Discussion

Micromechanical cantilever and doubly supported beams can be fabricated from poly-Si using a process that is compatible with MOS planar technology. This compatibility, the simple beam-fabrication process, and the piezoresistivity of poly-Si make these structures attractive for silicon micromechanics. In particular, an integrated sensor for organic vapors is being fabricated which incorporates a resonant poly-Si cantilever (7).

Two static properties of these beams have been investigated, the maximum length for a reliably free-standing beam, and the built-in deflection of cantilevers. The observed deflection is consistent with the presence of an internal bending moment which is plausible as the result of nonuniform internal stress across the poly-Si layer. Internal stress in a thin film arises from mismatches in thermal-expansion coefficients and from nucleation and growth phenomena (9). Annealing at 1100°C for 20 min before undercutting

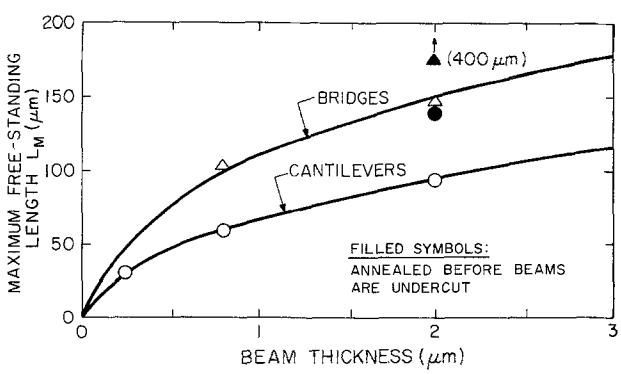


Fig. 7. Dependence of maximum free-standing length on beam thickness.

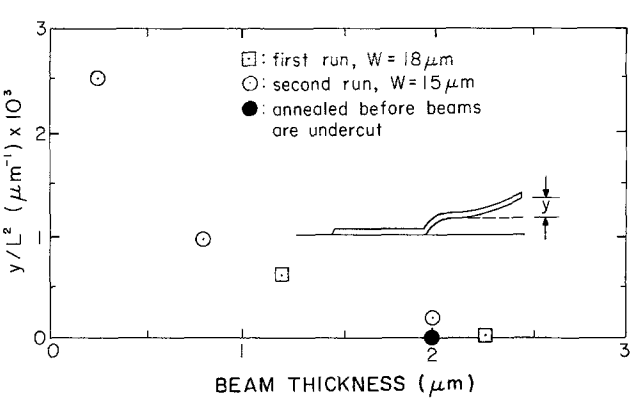


Fig. 8. Cantilever-tip deflection as a function of beam thickness

the beams with buffered HF increases the maximum free-standing length and eliminates the built-in deflection for beams shorter than $L_m$. This annealing procedure is sufficient to reflow the phosphosilicate glass layer underneath the poly-Si layer and cause recrystallization of the poly-Si, both of which may help to relax the nonuniform internal stress. Diffusion of phosphorus from the glass into the poly-Si will occur during this relatively severe anneal, which may be undesirable for certain applications. Additional research is needed to determine the minimum temperature and time required for stress relaxation in the poly-Si film. However, beams of useful sizes can be made without any post-deposition treatment of the poly-Si, as is demonstrated in Fig. 4-6. The dynamic properties of poly-Si micromechanical beams are currently being investigated, and the results will be reported later.

### Acknowledgments

We would like to thank Mrs. D. McDaniel for valuable laboratory assistance, and Dr. J. Shott of Stanford Integrated-Circuits Laboratory for use of a CVD oxide reactor. This work was supported by the National Science Foundation under grants ENG78-21854 and ECS-81-20562.

Manuscript submitted Aug. 16, 1982; revised manuscript received Feb. 14, 1983. This was Paper 118 presented at the Montreal, Que., Canada, Meeting of the Society, May 9-14, 1982.

Any discussion of this paper will appear in a Discussion Section to be published in the December 1983 JOURNAL. All discussions for the December 1983 Discussion Section should be submitted by Aug. 1, 1983.

REFERENCES

1. J. M. Jaffe, *Electron Lett.*, **10**, 420 (1974).
2. K. E. Petersen, *IEEE Trans. Electron Devices*, **ed-25**, 1241 (1978).
3. R. D. Jolly and R. S. Muller, *This Journal*, **127**, 2750 (1980).
4. K. E. Petersen and A. Shartel, *Tech. Digest IEDM*, 673 (1980).
5. J. C. North *et al.*, *IEEE Trans. Electron Devices*, **ed-25**, 809 (1978).
6. C. I. Drowley, Unpublished results.
7. R. T. Howe, M. S. Report, Dept. of Elect. Eng. and Comp. Sciences, Univ. of California, Berkeley, October 1981.
8. E. P. Popov, "Mechanics of Materials," 2nd ed., p. 361, Prentice-Hall, Englewood Cliffs, NJ (1976).
9. D. S. Campbell, in "Handbook of Thin Film Technology," L. I. Maissel and R. Glang, Editors, pp. 12-22, McGraw-Hill, New York (1970).

# A Study of the Diffusion of Oxygen in $\alpha$-Titanium Oxidized in the Temperature Range 460°-700°C

**D. David and G. Beranger**

*Laboratoire de Métallurgie et de Physicochimie des Matériaux, Universite de Technologie de Compiegne, B.P. 233, 60206 Compiegne Cédex, France*

**and E. A. Garcia**

*Comision Nacional de Energia Atomica, Dpto Materiales, Avda del Libertador 8250, 1429 Buenos Aires, Argentina*

ABSTRACT

The diffusion coefficient of oxygen in $\alpha$-titanium was measured in the range 460°-700°C, by means of nuclear microanalysis from the reaction $^{16}O(d,p)^{17}O^*$. A new application of this method allows the determination of a complete diffusion profile, along about 2 $\mu$m, from a single proton spectrum. The results provide a value of diffusion coefficient consistent with a bulk diffusion process, with an activation energy of 48 kcal/mol, over the temperature range from 200° to 950°C.

The high temperature oxidation of $\alpha$-titanium, with high current crystalline structure, gives a multilayered oxide film comprising several oxide species (1, 6). Moreover, a diffusion and dissolution of oxygen into the metal occurs under the oxide film, the oxygen atoms occupying the interstitial sites of the metal lattices. Thus, the oxygen concentration decreases continuously from the metal-oxide interface to the metal center. In order to understand the oxidation mechanism of titanium, it is necessary to analyze the two elementary mechanisms: growth of external oxides on one hand and formation of the oxygen-metal solid solution on the other hand.

Several investigations have been previously carried out on the oxygen diffusion phenomenon (2, 7-16). The values of the diffusion coefficient $D$ published by other authors shows a considerable scatter and hence in those for the activation energy, but this dispersion is perhaps related to the corresponding diversity in the experimental methods. The value previously mentioned were all obtained for temperatures higher than 650°C. For temperatures ranging between 250° and 400°C, other values of the oxygen diffusion coefficient were calculated from stress strain aging experiments (17, 18). It can be noted that the corresponding plots fit quite well with those of Ref. (16), which were obtained on the same material from experimental diffusion profiles. These values were directly measured, point by point, thus increasing their accuracy. Between 400°-650°C, there remains a temperature range where the diffusion coefficient values are unknown. However, two $D$ values for the temperatures of 420° and 490°C, have been obtained by Bertin (19) from calculations based upon internal friction measurements. Our results, and some others, are plotted in Fig. 1.

Thus, our purpose was to perform experiments in an intermediate temperature range, by means of a special application of nuclear microanalysis. The results obtained in this way cover the range from 460° to 700°C.

Key words: oxidation, diffusion, nuclear reactions, titanium.

### Experimental

Specimens of rolled Kroll titanium, containing 930 ppm of oxygen, were supplied by Cezus (Pechiney-Ugine-Kuhlmann) under the trademark UT 40. In order to determine the diffusion profiles, they were previously anodically oxidized, then heated under vacuum to permit oxygen diffusion. In this case, the oxide layer acts as an inexhaustible oxygen source and the concentrations on each side of the metal-oxide interface remain constant.

In the temperature range studied here (460°-700°C), the diffusion treatment times were selected in such a manner that the oxygen diffusion profiles into the metallic matrix should not exceed 2 $\mu$m in depth. The nuclear microanaly-